JBC Papers in Press. Published on September 9, 2009 as Manuscript C109.052159
The latest version is at http://www.jbc.org/cgi/doi/10.1074/jbc.C109.052159

MAL3 MASKS CATASTROPHE EVENTS IN *SCHIZOSACCHAROMYCES POMBE* MICROTUBULES BY INHIBITING SHRINKAGE AND PROMOTING RESCUE*

Miho Katsuki, Douglas R. Drummond, Michael Osei, and Robert A. Cross
From Molecular Motors Group, Marie Curie Reaerch Institute, Oxted, Surrey, RH8 0TL, UK
Running Title: *S. pombe* Mal3 Microtubule Dynamics
Address correspondence to: Robert A. Cross, The Chart, Oxted, Surrey, RH8 0TL,UK, Tel.: +44 1883 722 306 ex 219, Fax: +44 1883 714 375; E-mail: r.cross@mcri.ac.uk

Schizosaccharomyces pombe (S. pombe) **Mal3 is a member of the EB-family of proteins, which are proposed to be core elements in a tip-tracking network that regulates microtubule dynamics in cells. How Mal3 itself influences microtubule dynamics is unclear. We tested the effects of full length recombinant Mal3 on dynamic microtubules assembled in vitro from purified *S. pombe* tubulin, using dark-field video microscopy to avoid fluorescent tagging and data averaging techniques to improve spatiotemporal resolution. We find that catastrophe occurs stochastically as a fast (<2.2 secs) transition from constant-speed growth to constant-speed shrinkage with a constant probability that is independent of the Mal3 concentration. This implies that Mal3 neither stabilizes nor destabilizes microtubule tips. Mal3 does however stabilize the main part of the microtubule lattice, inhibiting shrinkage and increasing the frequency of rescues, consistent with recent models in which Mal3 on the lattice forms stabilizing lateral links between neighboring protofilaments. At high concentrations, Mal3 can entirely block shrinkage and induce very rapid rescue, making catastrophes impossible to detect, which may account for the apparent suppression of catastrophe by Mal3 and other EBs in vivo. Overall, we find that Mal3 stabilizes microtubules not by preventing catastrophe at the microtubule tip, but by inhibiting lattice depolymerization and enhancing rescue. We argue that this implies that Mal3 binds microtubules in different modes at the tip and on the lattice.**

Microtubules are intrinsically dynamic self-assembling structures of tubulin subunits (1) whose polymerisation is subject to extensive spatial and temporal control in cells partly through the activity of microtubule-associated proteins (2). In cells the EB family of microtubule plus-end tracking proteins (+TIPs) localises at the plus end of growing but not shrinking microtubules. EB depletion increases catastrophe frequency and reduces microtubule length in many species (3-5), suggesting EBs suppress microtubule catastrophes. It is however unclear from these cellular studies if this activity is direct or indirect since the dynamic binding of EBs to other +TIPs proteins enhances the localisation of all EB-complex proteins, including EB1, to microtubule ends (6).

To determine the direct effect of EB-family proteins on microtubule dynamics, in vitro experiments are necessary. These have established that microtubule end tracking is an intrinsic property of the EB proteins and that other +TIP proteins such as CLIP170 are dependent upon EBs for their microtubule end localisation (7-9). However EB1 binding also directly alters the structure of growing microtubule tips (10). In vitro studies show Mal3, the EB1-homologue in *Schizosaccharomyces pombe (S. pombe)* can also affect the structure of microtubules. Sandblad et al (11) found localisation of Mal3 along the (A-lattice) seam of B-lattice microtubules, and proposed this as a potential mechanism for direct microtubule stabilisation by the EBs. Des Georges et al showed that Mal3 binds to and specifically stabilises the A-lattice protofilament overlap, promoting nucleation and assembly of A-lattice-containing microtubules (12).

Several studies in vitro have all shown that EBs can affect microtubule dynamics (4,7,10,13), but conflict over which parameter is affected. So whilst Bieling et al and Manna et al observed no effect on microtubule growth rates, Komarova et al and Vitre et al found an acceleration of growth. Manna and colleagues found that EB1 inhibits catastrophe, yet the other studies observed that EBs trigger catastrophe events. There is clearly a need to resolve these apparent conflicts, especially as the same proteins in vivo appear to suppress catastrophe.

To try to elucidate the mechanism by which EB proteins influence microtubule assembly, we developed a minimalist approach in which the potential for confounding factors to affect the data is reduced or eliminated. Our assay uses proteins

from a single organism, *S. pombe* and GMPCPP-stabilised microtubule seeds assembled from purified tubulin with only the seeds attached to the chamber surface. We used this system to measure the effects of unlabeled full length Mal3 on the polymerisation dynamics of unlabeled *S. pombe* microtubules. Microtubules were imaged using dark-field microscopy to avoid fluorescent labelling (Fig. 1A). We also developed a semi-automated analysis system that allows us to digitise a large number of events, which can then be processed by data averaging and filtering. This reduces noise, allowing us to examine the detailed kinetics of the catastrophic switch from growth to shrinkage.

Using this system, we find that Mal3 has no direct effect upon the frequency or kinetics of catastrophe events, but that it does reduce shrinkage rates and increase rescue frequency in a dose-dependent manner.

EXPERIMENTAL PROCEDURES

Protein preparations--*S. pombe* single isoform tubulin and Mal3 protein (Mal3-308) were prepared and concentrations determined as described in des Georges et al (12). Pig brain tubulin was purified as described by Mitchison and Kirschner (14) and fluorescently labelled using Alexa Fluor 488 Succinimidyl Ester (A20000, Invitrogen) or Alexa Fluor 680 Succinimidyl Ester (A20008, Invitrogen) (15).

Microtubule dynamics assay--Polarity-marked GMPCPP microtubule seeds were attached by anti-Alexa 488 antibody (A11094, Invitrogen) to Sigma-cote (Sigma)-coated coverglasses in flow cells. Dynamic non-labelled *S. pombe* microtubules were assembled by addition of non-labelled 4.5 µM *S. pombe* single isoform tubulin in PEM buffer (100 mM Pipes, pH 6.9, 1 mM $MgSO_4$, 2 mM EGTA) (16) containing an oxygen-scavenging system (8 µg/ml catalase, 4.5 mg/ml glucose, 38 unit/ml glucose oxidase and 1% (v/v) 2-mercaptoethanol), 1 mM GTP and 1 mM Mg-ATP. Fluorescent seeds were imaged by epifluorescence microscopy and unlabeled microtubule dynamics by dark field microscopy in a temperature regulated box at 25 ± 0.5 °C. Dark field images were captured at 1 second intervals during a 30 minute incubation period using an electron-multiplying CCD camera (Andor, iXon^{EM}+ DU-897E).

Image analysis--Kymographs were created from time-lapse images of dynamic microtubules using MetaMorph software (Molecular Devices). Kymographs of microtubule plus ends (n = 8 - 32 from 3 - 5 microtubules for each condition) were analysed automatically using a custom macro for ImageJ (Rasband, W.S., ImageJ, U. S. National Institutes of Health, Bethesda, Maryland, USA, http://rsb.info.nih.gov/ij/, 1997-2009) that detects the microtubule end in dark-field kymograph images. This macro is available at http://mc11.mcri.ac.uk/motorhome.html.

Data processing--Catastrophe events were analysed by superimposing and aligning different data sets from the automated tip tracking using a custom Excel macro. A median filter was then applied to remove outlying data points and noise using a custom VBA macro in Excel. Macros are available at http://mc11.mcri.ac.uk/motorhome.html.

See Supplemental information for detailed methods.

RESULTS & DISCUSSION

We examined the effect of Mal3 expressed in *E. coli* on dynamic microtubules formed from highly purified single isoform *S. pombe* tubulin. Dynamic microtubules polymerised from immobilised, polarity-marked seeds assembled from pure tubulin, were imaged by dark-field microscopy (17) (Fig. 1B, Supplemental Movies). Kymographs were generated (Fig. 1C, D) and an automated tracking program developed to digitise the microtubule end position (Supplemental Method). Plots of microtubule end position against time were analysed to determine microtubule growth and shrinkage rates, catastrophe and rescue frequencies, which together define microtubule dynamics (Fig. 2A; Table 1). Measurements were repeated over a range of Mal3 concentrations.

We find that microtubules containing *S. pombe* single isoform tubulin grow at 0.5 µm/min (Fig. 2A; Table 1), compared to 3 µm/min in vivo (18). Addition of Mal3 at up to 500 nM does not alter this growth rate. Catastrophe frequency was determined from a large number of events (43-80 events during 103 -140 minutes of microtubule growth) and remained constant at 0.5 min^{-1} over the full range of Mal3 concentrations tested (Fig. 2A; Table 1).

Since Mal3 in vivo is reported to suppress catastrophe, we examined the intrinsic kinetics of

in vitro catastrophe in more detail, to determine if Mal3 alters the time course of catastrophe, rather than simply the frequency. For each Mal3 concentration, 8 – 32 subsets of catastrophe events suitable for further analysis were identified (Supplemental Table 1), excised from the primary data, superimposed and optimally aligned using a recursive procedure (Supplemental Methods). The final aligned data were median filtered to reduce noise (Supplemental Fig. S1). This image-processing procedure reveals the catastrophe event under unloaded conditions with unprecedented spatiotemporal resolution (Fig. 2B). Although Schek et al (19) previously tracked the dynamics of catastrophe at high resolution, their method requires exertion of force on the microtubule tip, which can alter the dynamics.

Our methods detect catastrophes as rapid transitions from steady growth to steady shrinkage with no intermediate states such as pauses, at all Mal3 concentrations assayed (Fig. 2B). By eye, transition from steady growth to steady shrinkage appears to occur within 1 second or so, at all concentrations of Mal3 (Fig. 2B). Plotting of the regions enclosing 95% of the data points for the median-filtered growth and shrinkage data provides a formal specification for the transition between growth and shrinkage (Supplemental Fig. S2). The overlap of these regions creates a zone around the catastrophe event where data points could belong to either growth or shrinkage regions or to some other transitional phase. The minimum physical extent we measure for this indeterminate zone is 64 nm (at 300 nM Mal3), whilst its minimum duration is 2.2 seconds (at 0 nM Mal3). These values represent upper limits for the spatiotemporal extent of the catastrophe zone.

Tip tracking by Mal3 on brain microtubules is observed in vitro in conditions similar to our assay (7). So although we do not directly visualise Mal3 we infer that tip tracking Mal3 does not affect either the frequency or the intrinsic dynamics of catastrophe in *S. pombe* microtubules.

Whilst Mal3 does not influence catastrophe frequency, it does have a considerable effect on plus end dynamics reducing shrinkage rates and increasing rescue frequencies following catastrophe (Fig. 2A; Table 1) in a dose dependent manner. Previously we showed that Mal3 binds the lattice of both brain and *S. pombe* microtubules with a 1:1 stoichiometry and K_d ~1 μM (12). We observe effects on shrinkage rates at Mal3 concentrations as low as 50 nM. With a K_d of 1 μM, Mal3 is predicted to occupy only about 4.6% of the lattice binding sites.

Mal3 increased the rescue frequency 6-fold over the range 0 to 500 nM Mal3 (Fig. 2A, Table 1). Rescues probably restore a protective cap of GTP tubulin heterodimers to the microtubule, blocking further shrinkage and allowing regrowth. Mal3 might directly promote the addition of GTP-heterodimers, however this mechanism seems unlikely, as we see no effect of Mal3 on the growth rate of microtubules assembling from GTP-heterodimers. Instead, we favour a model in which Mal3 is stabilising the GDP-lattice by linking protofilaments and inhibiting protofilament peeling, so that GTP-subunits can more easily add to the GDP-lattice microtubule end. Thus the same protofilament-linking mechanism could account for the ability of sparsely-distributed Mal3 to inhibit shrinkage and to promote rescues. Sparsely-distributed GTP-heterodimers within the lattice can also induce rescue events (20), potentially by a similar mechanism.

Mal3 tracks both the plus and minus ends of microtubules in vitro (7), and just as at the plus end, Mal3 at the minus end has no effect on growth rate, but slows shrinkage and promotes rescue, in a dose-dependent fashion (Fig. 2A; Table 1). However whilst Mal3 has no detectable effect on plus end catastrophe, it does appear to inhibit catastrophe at the minus end (Figs. 1C, 2A; Table 1; Supplemental Movie). Why does Mal3 apparently suppress catastrophe at minus ends but not at plus ends? Mal3 concentrations up to 100 nM do not inhibit the minus end catastrophe frequency, but higher Mal3 concentrations do and 500 nM Mal3 reduces the rate to zero (Fig. 2A; Table 1). Strikingly, the suppression of minus end catastrophe was only observed at concentrations of Mal3 (>300 nM) that significantly suppress minus end shrinkage rates (<1.0 μm/min) and promote minus end rescue (>8.2 min^{-1}) (Table 1). Inhibition of shrinkage and promotion of rescues requires more Mal3 at the plus end than at the minus end where the dynamics are already biased towards reduced shrinkage and increased rescues: even 500 nM of Mal3 only reduces plus end shrinkage rate to 5.7 μm/min and increases the rescue frequency to 4.1 min^{-1}.

We propose a model where Mal3 does not affect the catastrophe frequency itself. Instead, increasing Mal3 concentrations make catastrophes progressively harder to detect, by reducing the rate and duration of shrinkage events (Fig. 3A-C) until

it become essentially impossible to observe catastrophes. Our model envisages that the true catastrophe frequency is unaffected, even at high Mal3 concentrations, but that the *apparent* catastrophe frequency decreases.

Our model suggests that a sufficient increase in Mal3 concentration would cause the apparent suppression of all plus end catastrophes. We were unable to test this prediction directly in the dynamics assay as higher concentrations of Mal3 caused too much spontaneous nucleation of microtubules. So we used a protocol in which microtubules were pre-assembled and catastrophe events induced by reducing the free tubulin concentration (Supplemental Fig. S3). In the absence of Mal3, reducing the tubulin concentration from 7.5 μM to 3 μM resulted in immediate catastrophe followed by shrinkage to the stabilised seed boundary. However reducing the tubulin concentration to 3 μM in the presence of 1 μM Mal3 stabilised the microtubules for over 30 min in a paused state with no change in microtubule length or catastrophe events observable (Supplemental Fig. 3B). Subsequently flushing the chamber with 3 μM tubulin alone again caused immediate shrinkage (Supplemental Fig. 3C). Thus at high concentrations, Mal3 can suppress shrinkage and (apparently) suppress catastrophes at the microtubule plus end, consistent with our model. At the minus end, we observe continuous growth without catastrophes or pausing because of the combined effects of reduced shrinkage and increased rescue frequencies. The similar Mal3 dose-dependence of shrinkage rate reduction and rescue-promotion suggests that these effects may arise from the same mechanism. We propose that Mal3 linking of protofilaments stabilises the microtubule GDP-lattice, inhibiting shrinkage and promoting rescue leading to masking of catastrophe events.

Although like other EB-family proteins Mal3, enriches at the tips of growing microtubules (7), this higher concentration of Mal3 at microtubule ends compared to the lattice does not influence the dynamics of the microtubule end (Fig. 3D). We conclude that the Mal3 binding mode at the microtubule tip and on the lattice is different, perhaps because the tip is the only part of the microtubule composed of GTP heterodimers or because the tip is structurally different from the lattice (or both). It is paradoxical that the apparently higher affinity tip binding has no detectable effect on microtubule dynamics. One resolution of this paradox would be if Mal3 binding made GDP containing tubulin heterodimers behave more like GTP heterodimers, slowing their detachment from the microtubule whilst enhancing the probability of microtubule rescue by promoting attachment of GTP subunits. We previously proposed that the microtubule nucleating activity of Mal3 (12) could be explained by Mal3 binding and stabilising nascent sheets of heterodimers in a way analogous to its tip binding activity. Our present observations reveal that Mal3 does not stabilise tips, suggesting that the nucleating activity is more likely to arise from the lattice-stabilising activity that we observe here.

How do our observations apply in vivo? The concentration of Mal3 in cells may be about 200-fold less than the tubulin concentration (11). Based on our own preliminary estimates of tubulin concentration within *S. pombe* cells (not shown) the in vivo Mal3 concentration may be a few tens of nM, suggesting a potentially limited role for the direct effect of Mal3 on microtubule dynamics. To account for the observed stabilisation of growing microtubules by Mal3 in vivo, additional Mal3 binding partner proteins may be required to recruit sufficient Mal3 onto the lattice (13,21-23). Alternatively, the stabilisation of microtubules by Mal3 in vivo may be due to recruitment of Mal3 binding partners to the tips. Mal3 focuses to microtubule tips without affecting their dynamics – as such it provides a neutral platform for the recruitment of an extensive list of binding partners. Further in vitro reconstitution experiments will be necessary to test the relative contribution of these two mechanisms.

REFERENCES

1. Desai, A., and Mitchison, T. J. (1997) *Annu Rev Cell Dev Biol* **13**, 83-117
2. Akhmanova, A., and Hoogenraad, C. C. (2005) *Curr. Opin. Cell Biol.* **17**, 47-54
3. Busch, K. E., and Brunner, D. (2004) *Curr. Biol.* **14**, 548-559

4. Komarova, Y., De Groot, C. O., Grigoriev, I., Gouveia, S. M., Munteanu, E. L., Schober, J. M., Honnappa, S., Buey, R. M., Hoogenraad, C. C., Dogterom, M., Borisy, G. G., Steinmetz, M. O., and Akhmanova, A. (2009) *J. Cell Biol.* **184**, 691-706
5. Tirnauer, J. S., Grego, S., Salmon, E. D., and Mitchison, T. J. (2002) *Mol. Biol. Cell* **13**, 3614-3626
6. Akhmanova, A., and Steinmetz, M. O. (2008) *Nat Rev Mol Cell Biol* **9**, 309-322
7. Bieling, P., Laan, L., Schek, H., Munteanu, E. L., Sandblad, L., Dogterom, M., Brunner, D., and Surrey, T. (2007) *Nature* **450**, 1100-1105
8. Bieling, P., Kandels-Lewis, S., Telley, I. A., van Dijk, J., Janke, C., and Surrey, T. (2008) *J. Cell Biol.* **183**, 1223-1233
9. Dixit, R., Barnett, B., Lazarus, J. E., Tokito, M., Goldman, Y. E., and Holzbaur, E. L. (2009) *Proc. Natl. Acad. Sci. USA* **106**, 492-497
10. Vitre, B., Coquelle, F. M., Heichette, C., Garnier, C., Chrétien, D., and Arnal, I. (2008) *Nature Cell Biology* **10**, 415-421
11. Sandblad, L., Busch, K. E., Tittmann, P., Gross, H., Brunner, D., and Hoenger, A. (2006) *Cell* **127**, 1415-1424
12. des Georges, A., Katsuki, M., Drummond, D. R., Osei, M., Cross, R. A., and Amos, L. A. (2008) *Nature structural & molecular biology* **15**, 1102-1108
13. Manna, T., Honnappa, S., Steinmetz, M. O., and Wilson, L. (2008) *Biochemistry* **47**, 779-786
14. Mitchison, T., and Kirschner, M. (1984) *Nature* **312**, 232-237
15. Hyman, A., Drechsel, D., Kellogg, D., Salser, S., Sawin, K., Steffen, P., Wordeman, L., and Mitchison, T. (1991) *Methods Enzymol.* **196**, 478-485
16. Walker, R. A., O'Brien, E. T., Pryer, N. K., Soboeiro, M. F., Voter, W. A., Erickson, H. P., and Salmon, E. D. (1988) *J. Cell Biol.* **107**, 1437-1448
17. Horio, T., and Hotani, H. (1986) *Nature* **321**, 605-607.
18. Drummond, D. R., and Cross, R. A. (2000) *Curr. Biol.* **10**, 766-775
19. Schek, H. T., 3rd, Gardner, M. K., Cheng, J., Odde, D. J., and Hunt, A. J. (2007) *Curr. Biol.* **17**, 1445-1455
20. Dimitrov, A., Quesnoit, M., Moutel, S., Cantaloube, I., Pous, C., and Perez, F. (2008) *Science* **322**, 1353-1356
21. Browning, H., and Hackney, D. D. (2005) *J. Biol. Chem.*
22. Nakamura, M., Zhou, X. Z., and Lu, K. P. (2001) *Curr. Biol.* **11**, 1062-1067.
23. Mimori-Kiyosue, Y., Grigoriev, I., Lansbergen, G., Sasaki, H., Matsui, C., Severin, F., Galjart, N., Grosveld, F., Vorobjev, I., Tsukita, S., and Akhmanova, A. (2005) *J. Cell Biol.* **168**, 141-153

FOOTNOTES

*We gratefully acknowledge Cancer Research UK (C19638/A6211), Association for International Cancer Research (09-0221), Medical Research Council (G0200542) and Marie Curie Cancer Care for supporting this study.

Author contributions: MK developed the microtubule dynamics assay system, performed the experiments and wrote the analysis programs. DRD constructed the microscope combining dark-field and fluorescence illumination. MO purified *S. pombe* single isoform tubulin. MK, DRD and RAC planned experiments and wrote the paper.

The abbreviations used are: *S. pombe, Schizosaccharomyces pombe*; +TIPs, microtubule plus-end tracking proteins

FIGURE LEGENDS

FIGURE 1. In vitro *S. pombe* microtubule dynamics assay. (**A**) Schematic diagram of *S. pombe* microtubule dynamics assay. GMPCPP stabilised polarity-marked microtubule seed assembled from Alexa 488- and Alexa 680-labelled pig brain tubulin. Only the centre of the seed is attached to the surface

by anti-Alexa 488 antibody. Dynamic non-fluorescently labelled *S. pombe* microtubules grown from seeds were observed by dark-field illumination. (**B**) Merged Fluorescence images of GMPCPP stabilized, polarity-marked pig microtubule seed. Green: Alexa 488, Red: Alexa 680. Polarity is indicated by '-' or '+'. Plus end of seed has longer Alexa 680-labelled region (upper panel), Dark-field image showing pig microtubule seed plus elongated *S. pombe* microtubules (middle panel) and the merged images (lower panel). Red broken lines show ends of seed and yellow broken lines the ends of the elongated *S. pombe* microtubules. Arrows indicate the dynamic *S. pombe* microtubule elongated from the stabilised microtubule seed. Scale bar, 10 μm. (**C**) Kymographs of Microtubule length change over time. Left panel shows a diagram of a typical example. Time is vertical and length horizontal axis. Rescue (r) and catastrophe (c) events are labelled. Regrowth of shrinking microtubules from the seed (yellow arrow) were not counted as rescues. Scale bars; vertical 5 min, horizontal 20 μm. + and – ends of microtubule are indicated. (**D**) Enlargement of catastrophe events from yellow rectangle in (**C**). Scale bars; vertical 30 sec, horizontal 5 μm.

FIGURE 2. Mal3 effects on microtubule dynamics. (**A**) Microtubule plus and minus end dynamic parameters in 4.5 μM *S. pombe* tubulin and various concentrations of Mal3 (0 – 500 nM). Error bars: S.E.M. (**B**) Transition from growth to shrinkage during catastrophe events at plus ends in the presence of 0 - 500 nM Mal3. For each Mal3 concentration plots of microtubule length against time were superimposed and aligned by automated fits and the median determined. Error bars show upper and lower quartiles of the data. Scale bars: horizontal 10 sec, vertical 0.5 μm.

FIGURE 3. Model for microtubule binding modes and the apparent suppression of microtubule catastrophe events by Mal3 (**A**) In the absence of Mal3, growing microtubules undergo frequent catastrophe (red arrow) and shrink rapidly (violet arrow) with occasional rescues (blue arrow). (**B**) Sub-micro molar concentrations of Mal3 do not alter growth rate (green arrow) or catastrophe frequency (red arrow) but do slow shrinkage (violet arrow) and increase rescue frequency by lateral crosslinking of protofilaments. (**C**) At very high concentrations of Mal3, catastrophes still occur at the same rate, but become impossible to detect because the shrinkage rate is effectively zero whilst rescue events occur almost instantly. In all panels, longer coloured arrows indicate higher rate constants. (**D**) Mal3 binding modes. Mal3 has no effect on tip dynamics, but does affect lattice dynamics, implying two different binding modes. Mal3 binds with high affinity at the tip of growing microtubules giving rise to the characteristic EB-family comet. Catastrophe results in loss of tip-binding mode and exposure of the lattice. Mal3 binds with lower affinity on the lattice giving sparse decoration, but despite its lower affinity this lattice-bound Mal3 stabilises the lattice, forming lateral links between protofilaments and thereby slowing shrinkage and enhancing rescue. At sufficiently high concentrations of Mal3 these effects combine to give an apparent suppression of catastrophe events and continuous microtubule growth.

TABLE 1
Mal3 effect on microtubule dynamics

Data shows mean ± SD. Catastrophe events were defined as transitions between periods of continuous growth lasting longer than 20 seconds and periods of shrinkage longer than 3 seconds. Catastrophe and rescue frequencies were calculated by dividing the total number of events by the time spent in growth and shrinkage, respectively. n represents the total number of events observed. N/A not applicable (since no catastrophe events were observed)

Plus end

Mal3 (nM)	0	50	100	300	500
Growth rate (μm/min)	0.53 ± 0.13 n = 90	0.46 ± 0.20 n = 64	0.54 ± 0.15 n = 29	0.55 ± 0.21 n = 33	0.48 ± 0.13 n = 21
Shrinkage rate (μm/min)	11.4 ± 4.0 n = 21	10.1 ± 4.6 n = 39	7.8 ± 4.2 n = 10	5.2 ± 1.6 n = 34	4.1 ± 1.2 n = 20
Catastrophe frequency (events/min)	0.416 n = 53	0.567 n = 80	0.415 n= 43	0.659 n = 75	0.442 n = 54
Rescue frequency (events/min)	1.09 n = 4	1.14 n = 4	1.82 n= 5	2.96 n = 28	5.67 n = 48
Growth time (min)	127.40	141.08	103.50	113.75	122.08
Shrinkage time (min)	3.67	3.52	2.75	9.47	8.47

Minus end

Mal3 (nM)	0	50	100	300	500
Growth rate (μm/min)	0.19 ± 0.06 n = 32	0.14 ± 0.08 n = 29	0.13 ± 0.08 n = 23	0.17 ± 0.07 n = 5	0.15 ± 0.02 n = 4
Shrinkage rate (μm/min)	6.2 ± 5.7 n = 9	5.9 ± 1.7 n = 14	3.8 ± 5.3 n = 18	1.0 n = 2	N/A
Catastrophe frequency (events/min)	0.205 n = 28	0.264 n = 37	0.262 n= 30	0.07 n = 10	0
Rescue frequency (events/min)	3.43 n = 8	3.26 n = 5	4.36 n = 4	8.18 n = 3	N/A
Growth time (min)	136.43	140.32	114.37	143.18	137.82
Shrinkage time (min)	2.33	1.25	0.92	0.37	0.06

Figure 1

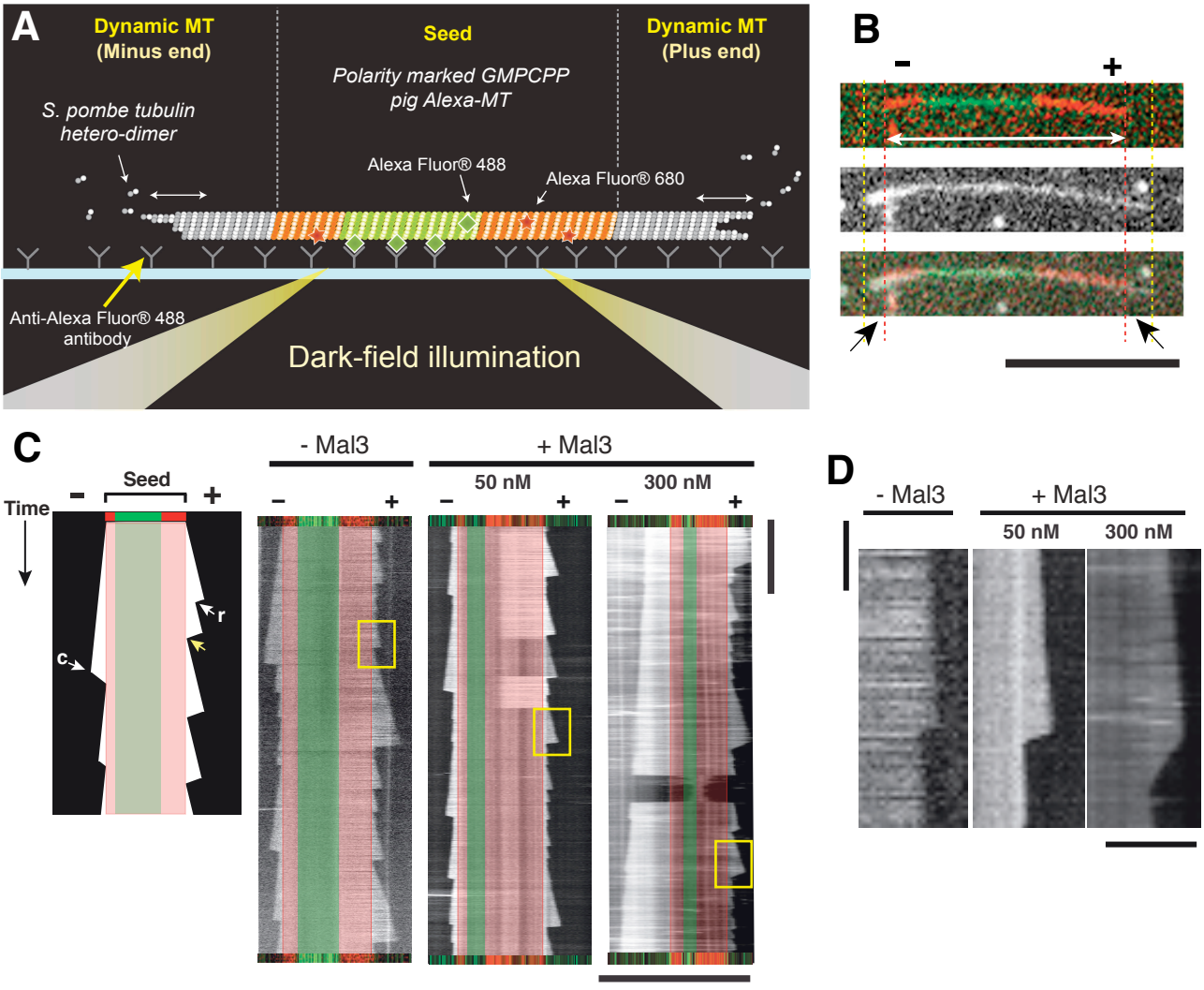

Figure 2

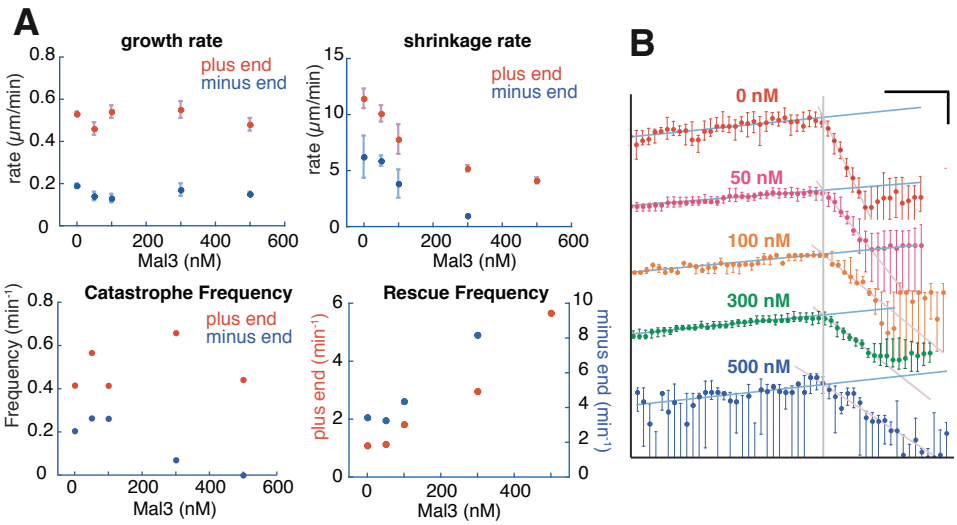

Figure 3